Unreliable homeostatic action potential broadening in cultured dissociated neurons

Andreas Ritzau-Jost[1,#], Salil Rajayer[2,3], Jana Nerlich[1], Filip Maciag[4], Alexandra John[1], Michael Russier[5], Victoria Gonzalez Sabater[6,7], Luke J. Steiger[2,3], Jacques-Olivier Coq[5], Jens Eilers[1], Maren Engelhardt[8,9], Juan Burrone[6,7], Dominique Debanne[5], Martin Heine[4], Stephen M Smith[2,3,#], Stefan Hallermann[1,#]

[1] Carl-Ludwig-Institute of Physiology, Faculty of Medicine, Leipzig University, Leipzig, 04103, Germany
[2] Division of Pulmonary and Critical Care Medicine, Department of Medicine, Oregon Health and Science University, Portland, Oregon, 97239-3098, USA
[3] Section of Pulmonary and Critical Care Medicine, VA Portland Health Care System, Portland, Oregon, 97239-2964, USA
[4] Institute for Developmental Biology and Neurobiology, Johannes Gutenberg University, Mainz, 55128, Germany
[5] Unité de Neurobiologie des canaux Ioniques et de la Synapse (UNIS), UMR_S 1072, INSERM, Aix-Marseille Université, Marseille, 13015, France
[6] MRC Centre for Neurodevelopmental Disorders, Institute of Psychiatry, Psychology and Neuroscience, King's College London, London, SE1 1UL, United Kingdom
[7] Centre for Developmental Neurobiology, Institute of Psychiatry, Psychology and Neuroscience, King's College London, London, SE1 1UL, United Kingdom
[8] Institute of Neuroanatomy, Mannheim Center for Translational Neuroscience, Medical Faculty Mannheim, Heidelberg University, Mannheim, 68167, Germany
[9] Institute of Anatomy and Cell Biology, Johannes Kepler University, Linz, 4020, Austria
[#] Correspondence: andreas.ritzau-jost@medizin.uni-leipzig.de (A.R-J.), smisteph@ohsu.edu (S.M.S.), and hallermann@medizin.uni-leipzig.de (S.H.)

Summary

Homeostatic plasticity preserves neuronal activity against perturbations. Recently, somatic action potential broadening was proposed as a key homeostatic adaptation to chronic inactivity in neocortical neurons. Since action potential shape critically controls calcium entry and neuronal function, broadening provides an attractive homeostatic feedback mechanism to regulate activity. Here, we report that chronic inactivity induced by sodium channel block does not broaden action potentials in neocortical neurons under a wide range of conditions. In contrast, action potentials were broadened in CA3 neurons of organotypic hippocampal cultures by chronic sodium channel block and in hippocampal dissociated cultures by chronic synaptic block. Mechanistically, BK-type potassium channels were proposed to underly inactivity-induced action potential broadening. However, BK channels did not affect action potential duration in our recordings. Our results indicate that action potential broadening can occur in specific neurons and conditions but is not a general mechanism of homeostatic plasticity in cultured neurons.

Introduction

Action potentials (APs) control various functions including neurotransmitter release from axonal boutons[1], calcium signals in the soma[2], and synaptic plasticity in dendrites[3]. AP broadening during short-term plasticity on the time scale of milliseconds to seconds is well-established and occurs in many types of neuronal cell bodies[4,5] and nerve terminals[6,7]. There are also indications that APs change during long-term plasticity on the time scale of minutes to hours. When examining Hebbian long-term plasticity (i.e., positive feedback-based and input-specific long-term plasticity[8]), some studies reported AP broadening. For example, presynaptic APs of hippocampal mossy fiber boutons broaden during depolarization-induced potentiation[9] and somatic APs of neurons in the amygdala broaden during fear conditioning[10]. In contrast, the role of the AP duration is less clear for non-Hebbian homeostatic long-term plasticity (i.e., negative feedback-based and non-input specific long-term plasticity[8]). Specifically, homeostatic plasticity induced by neuronal inactivity in the presence of the sodium channel blocker tetrodotoxin (TTX) has been studied for decades, but AP broadening was initially not described[11,12]. A recent study however reports prominent AP broadening during TTX-induced homeostatic plasticity at the soma of cultured neocortical neurons[13], which was not observed at presynaptic boutons of cultured neocortical neurons[14]. Compartmentalized AP broadening at the neuronal cell body would provide a strikingly simple and previously overlooked mechanism by which neuronal inactivity could increase subsequent excitability[13]. This mechanism involves decreased calcium entry during TTX application causing changes in gene expression that would result in broadened APs and more calcium entry after TTX removal. In this model, AP broadening is a key link in the homeostatic feedback loop underlying homeostatic plasticity. In a collaborative effort across several laboratories, we therefore systematically investigated AP broadening in cultured neurons during homeostatic plasticity under various experimental conditions.

Results

Cell type- and model-specific AP broadening in hippocampal neurons

APs in CA3 neurons of hippocampal organotypic slice cultures broaden homeostatically upon chronic inactivity using both, synaptic block by glutamate receptor antagonists[15] or sodium channel block by TTX[16] (see also ref. [17] for a similar

trend). We first aimed to confirm homeostatic AP broadening in CA3 neurons in organotypic slice cultures. APs were elicited by depolarizing currents from the resting membrane potential during perfusion with TTX-free artificial cerebrospinal fluid. APs recorded in CA3 pyramidal neurons treated with TTX (48 hours) had longer durations than those in control cells (Fig. 1A, B; median [IQR]: 1.75 [1.69–1.86] ms and 2.13 [2.07–2.22] ms for control and TTX-treatment, respectively, 14 cells each, $P < 0.001$), confirming earlier reports of homeostatic AP broadening in these neurons[15,16].

Next, we tested whether homeostatic AP broadening occurred in dissociated hippocampal cultured neurons, a model widely used to study homeostatic plasticity. We inhibited neuronal activity for 48 hours to induce homeostatic plasticity by either blocking AP firing using TTX (Fig. 1C) or by blocking synaptic transmission using the low-affinity glutamate receptor blocker kynurenic acid (Kyn) or the high-affinity glutamate receptor blocker 2,3-Dioxo-6-nitro-1,2,3,4-tetrahydrobenzo [f]quinoxaline-7-sulfonamide (NBQX). Surprisingly, AP duration was unaffected by TTX-treatment in primary hippocampal cultured neurons (Fig. 1D; median [IQR]: 2.07 [1.79–2.34] ms and 2.08 [1.32–2.61] ms for control and TTX, 25 and 24 cells, respectively, $P = 0.96$). In contrast, Kyn-treatment significantly increased AP duration in the same set of interleaved experiments (Fig. 1D; 2.52 [2.31–2.72] ms, 22 cells, $P = 0.014$) and NBQX-treatment led to a small trend towards broader APs (Fig. 1D; $P = 0.26$). Importantly, sodium channel block and synaptic block both increased spontaneous AP firing frequency, indicating that homeostatic adaptations other than AP broadening were shared between both induction methods (Fig. 1E, F; $P = 0.008$ for control against Kyn, $P = 0.005$ for control against NBQX, $P = 0.013$ for control against TTX). These data indicate that AP broadening occurred upon sodium channel block in CA3 neurons in organotypic slice cultures and upon synaptic block in dissociated hippocampal cultures, but not in the commonly-studied model of homeostatic plasticity using dissociated hippocampal cultured neurons and 48 hours of TTX application.

Stable AP duration in primary dissociated neurons during TTX-induced homeostatic plasticity

In contrast to our finding in dissociated cultured neurons of the hippocampus, a recent study described TTX-induced AP broadening in dissociated cultured neurons

of the neocortex[13]. To resolve this discrepancy, we set out to replicate AP broadening in neocortical cultured neurons. Given that exact reproduction of experimental conditions is challenging and neuronal plasticity depends on brain region[18], animal species[19], and animal strain[20], we probed homeostatic AP broadening under different experimental conditions varying: 1) experimental animal species (rat and mouse), 2) strain (C57BL/6 and CD1 mice), 3) sub-strain (C57BL/6N and C57BL/6J mice), 4) brain area (cortex and hippocampus), 5) cortical subdomain (prefrontal cortex), 6) culture duration (10–14, 15–21, and 32 days *in vitro*), 7) culture growth medium, 8) recording solutions, and 9) laboratory and experimenter performing recordings (conditions I–X in Fig. 2B, condition XI are recordings from Fig. 1; see also Fig. 2 – figure supplement 1). Even though AP durations varied up to 2-fold between conditions, homeostatic AP broadening was not detectable in any of the tested conditions (Fig. 2B). To detect cross-conditional AP broadening by TTX, we merged all conditions based on their difference in AP duration after TTX-treatment (Fig. 2C). However, AP duration was the same in control and TTX-treated cells (217 and 197 cells, respectively, $P = 0.83$).

We next tested whether AP broadening was concealed by systematic differences in neuronal health or recording quality between control and treatment group. We first analyzed AP amplitude as a measure of neuronal viability. AP amplitudes were not affected following TTX treatment in any of the eleven recording conditions (Fig. 2D) or a cross-conditional comparison (Fig. 2E). Next, neurons grown using a culture protocol or cortical subdomain previously associated with AP broadening were further analyzed to avoid the inclusion of inhibitory or depolarized neurons (ref. 13; conditions I, VII, and VIII). Inclusion criteria were the occurrence of multiple APs upon 200 ms-current injections (≥ 2 APs), a resting membrane potential below – 55 mV, and a maximum AP depolarization rate between 100 and 337 V/s (includes 96% of excitatory and exclude >80% of the inhibitory neurons; ref. 21). Applying any or all three of these criteria did not reveal AP broadening upon TTX treatment (Fig. 2 – figure supplement 2). These data indicate that stricter exclusion criteria result in smaller variability in action potential duration but do not uncover AP broadening in these datasets.

Instead of depolarization-evoked APs, Li *et al.*[13] recorded hyperpolarization-evoked 'rebound APs' (Fig. 2F), possibly reducing the impact of different resting membrane potentials and depolarizing current injection on the AP waveform. We determined that the duration of rebound APs was similarly unaffected by TTX treatment across several conditions (Fig. 2G, H). These data show that TTX-induced AP broadening does not robustly occur in dissociated cultured neurons.

Homeostatic plasticity increases network activity and excitatory synaptic transmission

To verify successful induction of homeostatic plasticity under our experimental conditions, we quantified changes in neuronal activity and synaptic strength following TTX-induced homeostatic plasticity. Spontaneously active neurons (Fig. 3A; merge of conditions I–IV and VII; control: 23 out of 87 cells, TTX-treatment: 58 out of 74 cells, $P < 0.001$ with Fisher's exact test) and the number of APs per spontaneous burst (Fig. 3B, C; median [IQR]: 1.0 [1.0–1.12] APs and 1.67 [1.0–2.71] APs for control and for TTX-treatment, 23 and 58 cells, respectively, $P < 0.001$) were increased after TTX-treatment. These results indicate an adaptive increase in neuronal activity following TTX-treatment, in line with previous findings on homeostatic plasticity[16,22,23]. Furthermore, spontaneous excitatory postsynaptic currents (sEPSCs; i.e., spontaneous synaptic currents recorded in the absence of TTX) were recorded as a measure of synaptic strength (Fig. 3D). sEPSC frequency and amplitude increased upon activity block by TTX (Fig. 2E, merge of recordings from condition I and II; median [IQR] frequency: 1.11 [0.42–1.47] Hz and 5.07 [1.95–5.52] Hz in control and TTX-treated cells, 16 and 11, respectively, $P = 0.027$; median [IQR] amplitude: 12.4 [10.6–14.4] pA and 15.5 [14.1–17.4] pA in control and TTX-treated cells, 16 and 11 cells, respectively, $P = 0.042$), in accord with known homeostatic synaptic adaptations to inactivity[24–27]. Taken together, blocking AP firing with TTX successfully induced homeostatic plasticity of excitability and synaptic strength under our experimental conditions.

Lack of BK channel-dependent AP broadening in dissociated cultured neurons

Various potassium channel subtypes regulate AP repolarization and could therefore underlie AP broadening. Li *et al.*[13] reported that downregulation of BK-type potassium channels led to homeostatic AP broadening in neocortical cultured neurons. We

tested the role of BK channels in AP repolarization (neurons grown under condition I). However, blocking BK channels with Iberiotoxin (IbTx, 300 nM) did not lead to broadening of depolarization-evoked APs in control and TTX-treated cells (Fig. 4A; P = 0.10 and 0.48, respectively), or a merge of both conditions (Fig. 4B; P = 0.10). Rebound APs were similarly unaffected by BK channel block (Fig. 4 – figure supplement 1). Next, we tested whether recurrent neuronal activity, which increases cytosolic calcium and boosts BK-channel activity, enhanced AP broadening following TTX treatment. While APs significantly broadened during repetitive firing, AP durations were similar in control and TTX-treated neurons (Fig. 4C and D), suggesting no differential regulation of BK-channels following TTX-treatment in these recordings.

In electrical recordings, intracellular recording solution may have disturbed cytosolic calcium dynamics and therefore BK- and thus calcium-dependent AP repolarization. As an independent approach, we recorded the AP duration in hippocampal cultured neurons using the genetically encoded voltage indicator (GEVI) Ace-mNeon[28] before and after acute IbTx perfusion (100 nM). BK channel block did not affect AP duration in the soma or along the axon (Fig. 4E). Using the GEVI, we again tested the role of BK channels in AP broadening during a train of APs (5 APs at 20 Hz, Fig. 4F). The broadening of somatic, proximal axonal, and distal axonal APs during trains was similar before and after BK channel block, indicating that AP duration was not modulated by BK channels. To confirm that IbTx was indeed pharmacologically active in Ace-mNeon recordings, we preconditioned cells with 4-AP (30 µM) prior to IbTx perfusion (Fig. 4G). Neurons preconditioned with 4-AP had broader somatic APs which were further broadened by IbTx, presumably due to increased calcium influx following 4-AP treatment, in turn activating more BK channels[29]. These data indicate that IbTx application was pharmacologically active but BK channels did not contribute to AP repolarization in cultured neocortical neurons.

Discussion

Homeostatic AP broadening has been reported in some systems, but it has not been tested systematically across experimental models so far. We found that AP broadening did not occur following the induction of homeostatic plasticity with TTX in the most commonly studied model system (primary dissociated neocortical neurons).

However, AP broadening was observed in cultured hippocampal slices. Furthermore, blocking BK channels, which were reported to mediate AP broadening during homeostatic plasticity[13], did not impact AP duration in dissociated cultured neurons. Our results therefore indicate that AP broadening in cultured dissociated neurons is not a required component of homeostatic plasticity.

TTX-induced homeostatic AP regulation in organotypic hippocampal cultured neurons

AP broadening was previously shown to occur in CA3 neurons of organotypic hippocampal slice cultures following TTX-induced homeostatic plasticity[16]. Consistently, we recorded broader APs in CA3 neurons following neuronal inactivity (Fig. 1). In contrast to CA3 neurons, granule cells of the dentate gyrus did not show TTX-induced AP broadening[17]. Similarly, CA1 neurons did not show AP broadening following synaptic block-induced homeostatic plasticity[30]. Therefore, homeostatic AP broadening is cell type-specific.

TTX-induced homeostatic AP regulation in primary dissociated cultured neurons

To the best of our knowledge, only three studies so far reported on the duration of APs following TTX-induced homeostatic plasticity in dissociated cultured neurons[13,31,32]. While Li *et al.*[13] observed TTX-induced broadening, the studies by Lee, Chung, and others[31,32] reported stable AP duration, consistent with our findings (Fig. 2). Furthermore, in other studies investigating TTX-induced homeostatic plasticity in dissociated cultured neurons, prominent AP broadening as observed by Li *et al.*[13] was either missed or absent, as in our recordings (see for example refs. [23,33–35]). One possible explanation for this inconsistency could be the cell type-specificity of AP broadening. We focused on large, presumably excitatory neurons. However, we and others could have selected different neuron types compared to Li *et al.*[13]. In an attempt to reduce bias, we incorporated multi-lab, randomization, and blinding strategies across many of our experiments. Only recordings with leaky seal formation or inadequate capacitance compensation[36] were excluded. AP amplitudes were unaffected by TTX treatment (Fig. 2). We then applied additional exclusion criteria to ensure that variability in neuronal type, health or recording quality were not causing a type II statistical error. Again, AP amplitudes were unaffected by TTX

treatment after excluding recordings with low resting membrane potential, with peak AP rates of depolarization outside the range for excitatory neurons, or those that did not fire repetitively (Fig. 2 – figure supplement 2). Even when these three criteria were applied together TTX failed to broaden AP duration, confirming that AP broadening was not associated with homeostatic plasticity in neocortical neurons following TTX treatment.

Synaptic block-induced homeostatic AP regulation in primary dissociated cultured neurons

Homeostatic AP broadening was shown in CA3 neurons upon activity block by the low-affinity glutamate receptor blocker Kyn[15]. We similarly observed Kyn-induced AP broadening in dissociated cultured hippocampal neurons (Fig. 1C, D). In contrast, APs were not significantly broader following synaptic block by NBQX (Fig. 1C, D). A differential effect of the glutamate receptor blockers Kyn and NBQX may relate to NMDA receptors, which are blocked by Kyn but not NBQX or TTX and which have recently been demonstrated to be important for the induction of synaptic homeostatic plasticity[37]. Further studies are needed to investigate the role of subcellular calcium signals in the regulation of AP duration during block of glutamate receptors.

Absence of BK channel-dependent AP broadening in dissociated cultured neurons

Li *et al.*[13] proposed that BK channels hasten AP repolarization and that this effect is lost during TTX-induced homeostatic plasticity, leading to AP broadening. We did not detect AP broadening when blocking BK channels in either control or TTX-treated cells (Fig. 4). Furthermore, APs did not broaden differentially during repetitive firing in control and TTX-treated neurons, suggesting no activity-dependent effect of TTX or BK channels on AP duration. Voltage imaging using Ace-mNeon similarly showed that width of single APs and broadening during AP trains in the soma and axon were unaffected by BK channel block. Blocking BK channels only affected AP repolarization when cells were preconditioned with 4-AP. These results are consistent with previous reports showing that in some neurons BK channels do not contribute to repolarization[38,39] while doing so in others[39–42]. Differences in the abundance of other types of potassium channels[39] and intracellular calcium buffering[41] are known to affect the contribution of BK channels to AP repolarization

and may account for the lack of AP broadening upon BK channel block in our dissociated cultured neurons. The lack of BK channel contribution to AP repolarization in our dissociated neurons is another possible explanation (in addition to different selection of cells) for why we and others have not observed the homeostatic AP broadening described by Li *et al.*[13].

Inactivity-induced homeostatic AP regulation *in vivo*

Homeostatic plasticity has also been studied using *in vivo* recordings from the activity-suppressed visual cortex[43,44]. The majority of these studies reported stable AP duration upon monocular deprivation or chemogenetic activity suppression[45–47]. In contrast, Li *et al.*[13] found homeostatically broadened APs in the visual cortex upon monocular deprivation. Furthermore, stable AP duration was also observed in other brain areas following activity suppression such as (1.) the somatosensory cortex upon unilateral whisker trimming[48–53] or forepaw denervation[54], (2.) the auditory system upon cochlear ablation[55,56], hearing loss[57], or congenital deafness[58], (3.) the vestibular nucleus upon vestibular ablation[59], and (4.) the olfactory mitral cells upon naris occlusion[60] or senescent hippocampal deafferentiation[61]. Besides somatic APs, APs in excitatory presynaptic terminals of the somatosensory thalamus were also unaffected by whisker deprivation[62]. Thus, AP broadening does not appear to occur robustly upon suppression of neuronal activity in various neuronal pathways.

Hyperactivity-induced homeostatic AP regulation

Homeostatic plasticity occurs not only upon activity block but also upon hyperactivity, generally involving opposite adaptations. In cultured neurons, AP duration was unaffected following hyperactivity induced by chronic depolarization[63], block of potassium channels[64], block of inhibitory synaptic transmission[30–32], or chronic ChR2-induced photostimulation[65]. In contrast, Li *et al.*[13] reported similar BK channel downregulation upon both, TTX-induced activity block and depolarization-induced hyperactivity.

As in cultured neurons, AP duration was mostly unaffected in brain slice recordings from animals with increased neuronal activity due to an enriched environment[53,66,67], psychosocial stress[68], or febrile seizures[69]. AP shortening occurred in cerebellar granule cells after exposure to an enriched environment[70], in auditory neurons

following chronic noise exposure[71], and in hippocampal neurons following age-related[72] or pilocarpine-induced hyperactivity[73]. Thus, in contrast to Li *et al.*[13], AP duration was either unaffected or, if anything, shortened during hyperactivity-induced homeostatic plasticity in previous studies.

In this study, several laboratories collaborated to determine the robustness of inactivity-induced AP broadening. AP broadening did not occur upon TTX-treatment in dissociated hippocampal or neocortical neurons. Furthermore, BK channel block did not affect AP duration in dissociated neurons, arguing against BK channels as mediators of homeostatic AP regulation.

METHODS

Ethics

At all times animal procedures were in accordance with the relevant international, national and institutional guidelines for the care and use of laboratory animals (European Council Directive 86/609/EEC, U.S. Public Health Service Policy on Humane Care and Use of Laboratory Animals, U.S. National Institutes of Health Guide for the Care and Use of Laboratory Animals, German Tierschutzgesetz, French National Research Council guidelines, and Leipzig and Mainz University guidelines). All animal procedures were approved in advance by the local health authorities (Ethics Committees at Leipzig University and Mainz University, federal Saxonian Animal Welfare Committee, the District administration Mainz-Bingen (41a/177-5865-§11 ZVTE), the Committee of the Préfecture des Bouches-du-Rhône (D13055-08), V.A. Portland Health Care System Institutional Animal Care and Use Committee).

Animal models

Organotypic hippocampal cultures were generated from postnatal day 5–7 Wistar rats.

Dissociated neocortical cultures were generated from postnatal day 0 or 1 Sprague-Dawley rats (conditions I, II and VII), C57BL/6N mice (conditions III and IV), C57BL/6J mice (conditions V and VIII), or CD1 mice (condition VI). Dissociated hippocampal cultures were generated from postnatal day 0 or 1 C57BL/6N mice (conditions IX), C57BL/6J mice (condition X), or Sprague-Dawley rats (condition XI).

Generally, animals of both sexes were used to generate cultures. Mother animals were kept in individually ventilated cages under a 12h/12h light-dark cycle and received water and food *ad libitum*.

Induction of Homeostatic Plasticity

Homeostatic plasticity was induced by inclusion of one of the respective blockers in culture medium for 48–56 hours prior to recordings. All blockers were first diluted in 100 µL of fresh medium per treated well and subsequently added to the respective wells containing 1 mL of medium. For control conditions, only 100 µL of fresh medium without blockers was added to the respective wells. The blockers had final concentrations of (in mM): 0.002 tetrodotoxin (TTX; Tocris, Wiesbaden-Nordenstadt, Germany), 2 kynurenic acid (Kyn), or 0.01 2,3-Dioxo-6-nitro-1,2,3,4-tetrahydrobenzo-[f]quinoxaline-7-sulfonamide (NBQX). To avoid bias, coverslips were randomized to treatment (control or blocker) and recordings were made and analyzed in a blinded fashion (except for condition IV and VI). Blinding was performed by an independent investigator. Control or TTX-treatment groups were assigned using an 8-block randomization approach for experiments of condition VIII. Unblinding of the experimental groups was performed after analysis and disclosure of the data by the experimenter.

Preparation of dissociated neocortical cultures

Conditions I and II (Hallermann Lab, Leipzig, Germany)

Neocortical cultures were generated as described by Li *et al.*[13]. Shortly, neocortices were isolated and dissected into 5–10 pieces per hemisphere. Samples were washed twice in ice-cold modified HBSS (4.2 mM $NaHCO_3$ and 1 mM HEPES, pH 7.35, 300 mOsm) supplemented with 20% fetal bovine serum (FBS) and digested at 37 °C for 30 min using papain. After stopping digestion with 20% FBS-containing modified HBSS, samples were washed and dissociated using Pasteur pipettes, pelleted twice, and filtered using a 70 nm nylon strainer. Dissociated cells were plated on poly-D-lysine-coated 14 mm coverslips and cultured in NbActive4 medium (Transnetyx, Cordova, TN, USA) in an incubator until use (37 °C, 5% CO_2 in room air, water vapor saturated).

Conditions III and VII (Hallermann Lab, Leipzig, Germany)

Cultures were generated as previously described by Moutin *et al.*[74]. In brief, mice were decapitated and neocortices (for condition III) or the frontal third of neocortices (for condition VII) were isolated in ice-cold Hibernate-A medium (Thermo Fisher Scientific, Waltham, MA, USA) and cut into 5–10 chunks. Chunks were first digested by papain (dissolved in Hibernate-A; 10 min at 37 °C) and subsequently by papain + DNAse (125 µL of 20 mg/mL DNAse stock; 5 min at 37 °C). Digestion was stopped by CM+ medium (Neurobasal A 86.5 %, B27 2 %, Glutamax 0.25 %, L-Glutamine 0.25%, penicillin G/streptomycin 1 %, heat-inactivated FBS 10 %) and chunks were mechanically dissociated in two steps by 1250 µL pipette tips with gravity decantation and collection of the supernatant between dissociation steps and after dissociation. Supernatant was passed through 2 mL of frothed bovine serum albumin, centrifuged (7 min, 300 x g), the resulting pellet was resuspended in 1–2 mL of CM+ medium and 25.000–30.000 resuspended cells were plated onto poly-L-lysine-coated coverslips. After 30 min, 0.5 mL of CM+ medium was added to the wells and after 2 days *in vitro* (DIV), cytosine arabinoside (ARA-C, 1 µM final concentration) was added to the wells for 8–18 h. Subsequently, 0.4 mL medium per well was replaced by fresh CM- medium (BrainPhys 96.75% by Stemcell Technologies, Vancouver, Canada, B27 2%, Glutamax 0.25%, penicillin G/streptomycin 1%) and further 0.1 mL of medium were exchanged every 6–7 days with fresh CM- medium until cells were used.

Condition IV (Hallermann Lab, Leipzig, Germany)

Cultures were generated following the protocol by Ritzau-Jost *et al.*[14]. In short, mice were decapitated and cerebral cortices were removed, dissected in ice-cold Hank's balanced saline solution, and cut into 5–10 pieces per hemisphere. Samples were digested by Trypsin (5 mg, dissolved in digestion solution; for composition see below) for 5 minutes at 37 °C. Trypsin was stopped by ice-cold MEM growth medium (composition see below), supernatant was discarded, and samples were mechanically and enzymatically dissociated using Pasteur pipettes of narrowing tip diameters in DNAse-supplemented MEM growth medium (10 mg/mL). The supernatant was centrifuged and the resulting pellet was resuspended in MEM growth medium for plating onto Matrigel-coated 14 mm coverslips (50.000 vital cells/coverslip). Forty-eight hours after plating, the medium was fully replaced by MEM growth medium containing 4 µM ARA-C to limit glial growth. After another 48 hours, the medium was fully replaced by MEM growth medium. Cells were incubated

at 37 °C, 93% humidity, and room air plus 5% CO_2 until use. Digestion solution contained the following (in mM): 137 NaCl, 5 KCl, 7 Na_2HPO_4, 25 HEPES, pH adjusted to 7.2 by NaOH. MEM growth medium was prepared from 1l MEM (Earle's salts + L-Glutamine) supplemented with 5 g Glucose, 0.2 g $NaHCO_3$, 0.1 g bovine holo-Transferrin, 0.025 g bovine insulin, 50 mL FBS and 10 mL B-27.

Conditions V, VI and VIII (Smith Lab, Portland, OR, USA)

Cultures were generated following the protocol by Martiszus *et al.*[75]. Briefly, 1–2-day old mice were decapitated following general anesthesia with isoflurane, and their cerebral cortices (for conditions V and VI) or the frontal third of neocortices (for condition VIII) were dissected out while bathed in ice-cold modified Hank's balanced saline solution (modified HBSS; Hyclone laboratories, Logan, UT, USA) and cut into 5–10 pieces per hemisphere. Samples were digested by Trypsin (10 mg, dissolved in digestion solution as mentioned in Condition IV) for 5 minutes at 37 °C. Trypsin was de-activated by ice-cold HBSS with 20% FBS, supernatant was discarded, and samples were enzymatically and mechanically dissociated using Pasteur pipettes with narrowing tip diameters in DNAse-supplemented HBSS. The supernatant was centrifuged and the resulting pellet was resuspended in 5% MEM growth medium (see composition above in Condition IV) for plating onto Matrigel-coated 12 mm glass coverslips. MEM growth medium containing 4 µM ARA-C was added 48 hours later to limit glial proliferation, and subsequently replaced with MEM growth medium following another 48 hours. Cells were incubated at 37 °C, 93% humidity, and room air plus 5% CO_2 until use between days 11–14 *in vitro.*

Preparation of dissociated hippocampal cultures

Condition IX and X (Heine Lab, Mainz, Germany)

In short, mice pups were decapitated and brains were removed. Hippocampi were dissected in ice-cold Hank's balanced saline solution and digested by trypsin for 15 minutes at 37 °C. Next, the tissue was washed with cold HBSS and mechanically dissociated using Pasteur pipettes in DNAse-, glutamate- and FBS-supplemented DMEM growth medium. 100 µL of cell suspension containing approximately 70.000 cells was placed on a glass coverslip and incubated at 37 °C, 5% CO_2 for 1 hour. Coverslips were then transferred to 12-well plates with glutamate-, B27- and sodium pyruvate-supplemented Neurobasal A medium (1 mL per well) and cultivated until

use. Double distilled water was added in between the wells of the 12-well plate to prevent evaporation of the medium during cultivation.

Condition XI (Hallermann Lab, Leipzig, Germany)

Cultures were generated as described for Condition III, except that hippocampi from postnatal day 0–1 Sprague-Dawley rats were used for preparation.

Recordings from dissociated cultures

Within conditions, recordings were performed blinded (except conditions IV and VI) and interleaved from randomized sister coverslips of the same culture, at the same recording setup, and by the same experimenter.

Conditions I – IV, VII and XI (Hallermann Lab, Leipzig, Germany)

Voltage- and current-clamp recordings were performed with borosilicate pipettes using a HEKA EPC10/2 amplifier (HEKA Elektronik, Lambrecht/Pfalz, Germany). Borosilicate glass tubes (Science Products, Hofheim, Germany) were pulled by a DMZ Universal Electrode Puller with filament heating (Zeitz Instruments, Martinsried, Germany) to 3–6.5 MΩ pipette resistance. Pipettes were filled with internal solution (see *Solutions and reagents* section) and mounted on a micromanipulator (Kleindiek Nanotechnik, Reutlingen, Germany) using a custom-built pipette holder. Recordings were performed at room temperature (22–25 °C). All current-clamp recordings were filtered with the internal 10 kHz 8-pole Bessel filter of the HEKA EPC10/2 amplifier and subsequently digitized (200 kHz) with the HEKA EPC10/2 using Patchmaster software (HEKA Elektronik, Lambrecht/Pfalz, Germany). Built-in compensation was used for voltage offset and pipette capacitance. Membrane potentials were not corrected for liquid junction potential and bridge compensation was adjusted to minimize the current injection artifact. APs were evoked by brief 1 ms depolarizing current injections of 500–1500 pA or 500 ms hyperpolarizing pulses (300–1000 pA) leading to APs upon return to resting membrane potential (‘rebound APs’). Both, depolarization-evoked and rebound APs were first recorded at resting membrane potential without holding current. While depolarization readily evoked APs in all conditions, rebound AP did not occur in all conditions at their resting membrane potential. In these cells, holding currents were used to depolarize cells until rebound APs were observed upon long hyperpolarizing pulses. Spontaneous excitatory

postsynaptic currents were recorded in voltage-clamp mode at -70 mV membrane potential in neurons grown in conditions I and II. Currents were filtered with the internal 3 kHz 8-pole Bessel filter of the HEKA EPC10/2 amplifier, digitized (200 kHz) and detected using the template matching algorithm [76] implemented in NeuroMatic (Version 2.00, 15.09.2008; ref. [77]).

Conditions V, VI and VIII (Smith Lab, Portland, OR, USA)

Current-clamp recordings were performed with borosilicate pipettes using a HEKA EPC10 amplifier (HEKA Elektronik, Lambrecht/Pfalz, Germany). Patch pipettes (5–10 MΩ resistance) were pulled from thin-walled borosilicate glass tubes (Warner Instruments, Holliston, MA, USA) using a P-87 electrode puller (Sutter Instruments, Novato, CA, USA). Pipettes were filled with an internal solution (see *Solutions and reagents* section) and mounted on a micromanipulator (ROE-200, Sutter Instruments, Novato, CA, USA). Recordings were performed at room temperature (22–25 °C). Voltage signals were filtered at 2.9 kHz and digitized at 20 kHz. Membrane potentials were corrected for liquid junction potential and bridge balance was performed manually prior to data acquisition. All APs were evoked by a sequence of transient injections relative to the resting membrane potential and measurements taken from the APs elicited with the minimal stimulus using either depolarizing current injections (500–1000 pA in 100 pA increments for 1–3 ms in 0.5 ms increments in conditions V and VI or 20–140 pA in 20 pA increments for 0.5 s in condition VIII) or following rebound from longer hyperpolarizing pulses (300–1200 pA in 100 pA increments for 500 ms).

Conditions IX & X (Heine Lab, Mainz, Germany)

Voltage- and current-clamp recordings were performed with borosilicate pipettes using a HEKA EPC9 amplifier (HEKA Elektronik, Lambrecht/Pfalz, Germany). Filamented glass tubes (Science Products, Hofheim, Germany) were pulled by a Narishige PC-100 electrode puller. Resistance of the pipettes was 2–6 MΩ. Pipettes were filled with internal solution (see *Solutions and reagents* section) and mounted on a micromanipulator (Luigs & Neumann, Ratingen, Germany). Recordings were performed at room temperature (21–24 °C). Signals were filtered at 2.9 kHz and digitized at 20 kHz using Patchmaster software (HEKA Elektronik, Lambrecht/Pfalz, Germany). Built-in compensation was used for voltage offset and pipette

capacitance. Membrane potentials were not corrected for liquid junction potential. APs were evoked by brief 1 ms depolarizing current injection of 50–300 pA or 500 ms hyperpolarizing pulses (300–400 pA) leading to APs upon return to resting membrane potential ('rebound APs').

Preparation of organotypic hippocampal cultures

Cultures were prepared as described previously[78]. In brief, young Wistar rats (P5–P7) were anesthetized with isoflurane and killed by decapitation, the brain was removed, and each hippocampus was dissected. Hippocampal slices (350 µm) were obtained using a Vibratome (Leica, VT1200S, Wetzlar, Germany). They were placed on 20 mm latex membranes (Millicell; Merck, Darmstadt, Germany) inserted into 35 mm Petri dishes containing 1 mL of culture medium and maintained for up to 8 days in an incubator at 34 °C, 95% O_2, 5% CO_2. The culture medium contained 25 mL MEM, 12.5 mL HBSS, 12.5 mL horse serum, 0.5 mL penicillin/streptomycin, 0.8 mL glucose (1 M), 0.1 mL ascorbic acid (1 mg/mL), 0.4 mL HEPES (1 M), 0.5 mL B27, and 8.95 mL sterile H_2O. To limit glial proliferation, 5 µM ARA-C was added to the culture medium starting at DIV 4.

AP recordings from organotypic hippocampal cultures

Whole-cell recordings were obtained from CA3 neurons in organotypic cultures at DIV 7 to DIV 10. All recordings were made at 34 °C in a temperature-controlled recording chamber (Luigs & Neumann, Ratingen, Germany) using 7–10 MΩ patch pipettes. CA3 pyramidal neurons were recorded in current-clamp with a Multiclamp 700B Amplifier (Molecular Devices, San Jose, CA, USA). APs were elicited by delivering DC step pulses (duration 1.0 s) at an interstimulus interval of 10–15 s. During the whole recording, ionotropic glutamate and $GABA_A$ receptors were blocked with 2–4 mM kynurenic acid and 100 µM picrotoxin, respectively.

Analysis of APs

Data were analyzed using IGOR PRO software (WaveMetrics, Lake Oswego, OR, USA; Version 6.32A or 6.37), the Patcher's Power Tool (Version 2.19 Carbon, 15.03.2011) and NeuroMatic (Version 2.00, 15.09.2008; ref. [77]) extensions, as well as self-written IGOR PRO scripts. AP durations were quantified as the duration at half-maximal AP amplitude, amplitude being the difference between AP peak and the

membrane potential preceding stimulation. When AP durations were recorded at half-maximal amplitude between AP threshold (defined as the membrane potential at which the voltage rate of change first reaches 10 V/s) and AP peak, AP durations were still unaffected by TTX treatment (data not shown). To exclude the effect of mis-balanced bridge compensation on AP shape, only APs that occurred after the end of the second current injection artifact (elicited by the end of current-injection) were analyzed. In some recordings, current injection artifacts were blanked over 50 µs at the beginning and the end of the current injection and only experiments in which blanking did not affect AP amplitude and duration were subsequently analyzed.

Hippocampal dissociated cultures and transfection for GEVI imaging

Culture preparation and GEVI transfection were performed as previously described by Sabater *et al.*[28]. In short, hippocampi were dissected from embryonic day 17.5 Wistar rat pups of either sex, treated with trypsin (Worthington Biochemical Corporation, Lakewood, NJ, USA) at 0.5 mg/mL, and mechanically dissociated using fire polished Pasteur pipettes. Neurons were plated on 18 mm glass coverslips pre-treated with 100 µg/mL poly-L-lysine and coated with 10 µg/mL laminin (Thermo Fisher Scientific, Waltham, MA, USA). Cultures were maintained in Neurobasal medium with B27 (1x) and GlutaMAX (1x, all obtained from Thermo Fisher Scientific, Waltham, MA, USA), supplemented with FBS (2%, Biosera, Nuaille, France) and Penicillin/Streptomycin (1%, Sigma-Aldrich, St. Louis, MO, USA), at 37°C in a humidified incubator with 5% CO_2. For transfections with Ace2N-mNeon-4AA (Ace-mNeon, ref. [79]; distributed by Biolife Solutions Inc., Bothell, WA, USA), the Effectene transfection reagent (Qiagen, Venlo, Netherlands) was used. The medium was changed at DIV 3 to culture medium without antibiotic or FBS, and transfections with Effectene were performed at DIV 7 following the manufacturer's protocol. After transfection neurons were maintained in serum-free media without antibiotics. For all experiments 30% of the medium was changed weekly and neurons were imaged 7–14 days after transfection (14–21 DIV).

GEVI Imaging conditions

GEVI imaging was performed as previously described by Sabater *et al.*[28]. In short, neurons were imaged using an inverted Olympus IX71 epifluorescence microscope with a 60x 1.42 NA oil-immersion objective (Olympus, Tokyo, Japan). Coverslips

were mounted in a heated chamber (Warner instruments, Holliston, MA, USA; total volume ~500 µL) and placed on an IMTP microscope stage (Scientifica, Uckfield, United Kingdom). Cells were maintained in external HEPES-buffered saline solution (HBS: 2 mM $CaCl_2$, 1.6 mM $MgCl_2$, 1.45 mM NaCl, 2.5 mM KCl, 10 mM Glucose, 10 mM HEPES, pH 7.4, Osmolarity 290 mOsm) and experiments were carried out at near physiological temperatures of 32–35 ºC.

In Ace-mNeon imaging experiments, ~505 nm excitation illumination was provided using a 525 nm LED (Solis LED, Thorlabs, Newton, NJ, USA), a 500/20 nm excitation filter, and a 510 nm long-pass dichroic mirror. Ace-mNeon emission transmitted through the dichroic was filtered using a 520 nm long-pass filters (Chroma, Bellows Falls, VT, USA). A power density of 10 mW/mm^2 was obtained at the specimen plane. Images were acquired at 3.2 kHz with an ORCA-Flash4.0 V2 C11440-22CU scientific CMOS camera (Hamamatsu Photonics, Hamamatsu, Japan) cooled to ~ -20 ºC with the Exos2 water cooling system (Koolance, Auburn, WA, USA). Images were acquired with HCImage software (Hamamatsu, Hamamatsu, Japan), binned to 4 × 4 and cropped to a 16 × 512-pixel region of interest, necessary to achieve the high image acquisition rates. Images were saved in CXD format.

Stimulation of APs was achieved with an extracellular tungsten parallel bipolar electrode (FHC, Bowdoin, ME, USA) mounted on a PatchStar motorized micro-manipulator (Scientifica, Uckfield, United Kingdom). To reliably induce an AP, we delivered a 1 ms 10 mV pulse at the soma. The timing of the LED illumination, the acquisition and stimulation were triggered externally through Clampex software (pClamp 10, Molecular Devices, San Jose, CA, USA).

All GEVI Imaging recordings were performed in presence of NBQX (10 µM), Gabazine (10 µM) and D-2-amino-5-phosphonovalerate (APV, 25 µM; all from Bio-Techne, Wiesbaden-Nordenstadt, Germany) in order to block synaptic transmission and ensure that the observed events were due to the stimulation only. IbTx was delivered using a custom gravity-fed perfusion system and bath volume was maintained by a peristaltic pump (Watson-Marlow 120s; Watson-Marlow, Rommerskirchen, Germany).

Image analysis

Image analysis was performed as previously described by Sabater *et al.*[28]. In short, voltage imaging recordings were analyzed in ImageJ and custom scripts within MATLAB software as follows. Prior to analysis, if drift had occurred in the x and y axis during the recording, the images were aligned using the TurboReg ImageJ plugin[80]. Images were then imported into MATLAB and fluorescence intensity profiles were obtained from regions of interest (ROIs) manually drawn around neuronal structures identified visually on a maximum projection image of the time series by averaging across the ROI pixels in each frame. The fluorescence profile was separated into single trials and corrected for background camera noise by subtracting the average intensity value of the timepoints where no illumination light was applied. Then, recordings were reconstructed at a sampling rate of 100 kHz using cubic spline interpolation. Bleaching was estimated by fitting a single exponential function to each individual trace smoothed using an averaging filter with a window of 3 and interpolated. The resulting curve was used to correct an unfiltered interpolated version of the recording. An accurate representation of the AP waveform with an enhanced SNR was obtained by averaging over the repeats and extracting the AP parameters from the resulting trace. The fluorescence profile during the 20 ms preceding a response was used as baseline.

Solutions and reagents

Reagents were purchased from Sigma-Aldrich (St. Louis, MO, USA) if not indicated otherwise.

Conditions I, II, VII and XI

The extracellular bath solution contained (in mM): 122 NaCl, 3 KCl, 10 D-Glucose, 26 $NaHCO_3$, 1.25 Na_2HPO_4, 1.3 $MgCl_2$, and 2.0 $CaCl_2$. After equilibration with 95% O_2–5% CO_2, pH was adjusted to 7.35 if needed by NaOH or HCl. The intracellular pipette solution contained (in mM): 130 K gluconate, 1 $MgCl_2$, 10 HEPES, 0.3 EGTA, 10 Tris-Phosphocreatine, 4 Mg-ATP, 0.3 Na-GTP. When testing the contribution of BK channels, 300 nM Iberiotoxin (Abcam, Cambridge, United Kingdom) was included in the bath solution.

Conditions III and IV

The extracellular bath solution contained (in mM): 125 NaCl, 3 KCl, 25 Glucose, 25 $NaHCO_3$, 1.25 Na_2HPO_4, 1.1 $MgCl_2$, and 1.1 $CaCl_2$. After equilibration with 95% O_2–5% CO_2, pH was adjusted to 7.35 if needed by NaOH or HCl. The intracellular pipette solution contained (in mM): 150 K Gluconate, 10 K-HEPES, 3 Mg-ATP, 0.3 Na-GTP, 0.05 EGTA, 10 NaCl.

Conditions V and VI

The extracellular bath solution contained (in mM): 150 NaCl, 4 KCl, 10 HEPES, 10 glucose, 1.0 $MgCl_2$, and 2.0 $CaCl_2$, and was equilibrated with 95% O_2–5% CO_2. The intracellular pipette solution contained (in mM): 135 K gluconate, 4 NaCl, 0.05 EGTA, 10 HEPES, 3 $MgCl_2$, 0.3 NaGTP, 3 Na_2ATP, 10 Na_2-Creatine phosphate with pH normalized to 7.25 using KOH.

Condition VIII

The extracellular bath solution contained (in mM): 122 NaCl, 3 KCl, 1.25 NaH_2PO_4, 26 $NaHCO_3$, 10 glucose, 1.3 $MgCl_2$, and 2.0 $CaCl_2$, and was bubbled with 95% O_2–5% CO_2. The intracellular pipette solution contained (in mM): 130 K gluconate, 0.3 EGTA, 10 HEPES, 2 $MgCl_2$, 0.3 NaGTP, 4 Na_2ATP (or Mg-ATP), 10 Na_2-Creatine phosphate (or Tris-Creatinine phosphate).

Conditions IX and X

The extracellular bath solution contained (in mM): 145 NaCl, 2.5 KCl, 10 HEPES, 24 glucose, 1.3 $MgCl_2$, and 2.0 $CaCl_2$, and was equilibrated with 95% O_2–5% CO_2. The intracellular pipette solution contained (in mM): 140 K gluconate, 2 NaCl, 0.5 EGTA, 20 HEPES, 3 $MgCl_2$, 0.3 NaGTP, 4 Na_2ATP, with pH adjusted to 7.25 using KOH.

Organotypic hippocampal neuron recordings

The external bath solution contained (in mM): 125 NaCl, 26 $NaHCO_3$, 3 $CaCl_2$, 2.5 KCl, 2 $MgCl_2$, 0.8 NaH_2PO_4, and 10 D-glucose, and was equilibrated with 95% O_2–5% CO_2. The intracellular pipette solution contained (mM): 120 K gluconate, 20 KCl, 10 HEPES, 0.5 EGTA, 2 $MgCl_2$, 2 Na_2ATP, and 0.3 NaGTP (pH 7.4).

Statistics

If not otherwise noted, data are expressed as box plots with boxes reflecting 25th–75th percentile. The median is indicated by a line within the box, whiskers indicate 10th and 90th percentile. Sample sizes (n) provide the number of individual somatic recordings. All data sets were obtained from ≥ 2 independent cell cultures. Data in Fig. 3A were tested for statistical difference using Fisher's exact test. Confidence limits for 95% confidence intervals were calculated as Wilson interval[81]. Other experimental groups were independent and tested by the Mann-Whitney *U* test. Tests were performed in IGOR PRO or GraphPad Prism 8. Results were considered significant at $p < 0.05$.

Acknowledgment

This work was supported by a European Research Council Consolidator Grant (ERC CoG 865634) the German Research Foundation (HA6386/10-2) to S.H. and by grants awarded by the U.S. Department of Veterans Affairs (BX002547) and NIGMS (GM134110) to S.M.S.

Declaration of interests

The authors declare no competing interests.

References

1. Borst, J.G.G., and Sakmann, B. (1999). Effect of changes in action potential shape on calcium currents and transmitter release in a calyx-type synapse of the rat auditory brainstem. Philosophical Transactions of the Royal Society B: Biological Sciences *354*, 347–355. https://doi.org/10.1098/RSTB.1999.0386.
2. Christie, B.R., Eliot, L.S., Ito, K.I., Miyakawa, H., and Johnston, D. (1995). Different Ca2+ channels in soma and dendrites of hippocampal pyramidal neurons mediate spike-induced Ca2+ influx. J Neurophysiol *73*, 2553–2557. https://doi.org/10.1152/jn.1995.73.6.2553.
3. Watanabe, S., Hoffman, D.A., Migliore, M., and Johnston, D. (2002). Dendritic K+ channels contribute to spike-timing dependent long-term potentiation in hippocampal pyramidal neurons. Proc Natl Acad Sci U S A *99*, 8366–8371. https://doi.org/10.1073/PNAS.122210599.
4. Bean, B.P. (2007). The action potential in mammalian central neurons. Nat Rev Neurosci *8*, 451–465. https://doi.org/10.1038/nrn2148.
5. Debanne, D., Campanac, E., Bialowas, A., Carlier, E., and Alcaraz, G. (2011). Axon physiology. Physiol Rev *91*, 555–602. https://doi.org/10.1152/PHYSREV.00048.2009.
6. Geiger, J.R.P., and Jonas, P. (2000). Dynamic control of presynaptic Ca2+ inflow by fast-inactivating K+ channels in hippocampal mossy fiber boutons. Neuron *28*, 927–939. https://doi.org/10.1016/S0896-6273(00)00164-1.
7. Jackson, M.B., Konnerth, A., and Augustine, G.J. (1991). Action potential broadening and frequency-dependent facilitation of calcium signals in pituitary nerve terminals. Proc Natl Acad Sci U S A *88*, 380–384. https://doi.org/10.1073/PNAS.88.2.380.
8. Keck, T., Toyoizumi, T., Chen, L., Doiron, B., Feldman, D.E., Fox, K., Gerstner, W., Haydon, P.G., Hübener, M., Lee, H.K., et al. (2017). Integrating Hebbian and homeostatic plasticity: The current state of the field and future research directions. Philosophical Transactions of the Royal Society B: Biological Sciences *372*. https://doi.org/10.1098/rstb.2016.0158.
9. Carta, M., Lanore, F., Rebola, N., Szabo, Z., Da Silva, S.V., Lourenço, J., Verraes, A., Nadler, A., Schultz, C., Blanchet, C., et al. (2014). Membrane lipids tune synaptic transmission by direct modulation of presynaptic potassium channels. Neuron *81*, 787–799. https://doi.org/10.1016/J.NEURON.2013.12.028.
10. Senn, V., Wolff, S.B.E., Herry, C., Grenier, F.O., Ehrlich, I., Grü, J., Fadok, J.P., Müller, C., Letzkus, J.J., and Lüthi, A. (2014). Long-range connectivity defines behavioral specificity of amygdala neurons. Neuron *81*, 428–437. https://doi.org/10.1016/j.neuron.2013.11.006.
11. Turrigiano, G.G., and Nelson, S.B. (2004). Homeostatic plasticity in the developing nervous system. Nat Rev Neurosci *5*, 97–107. https://doi.org/10.1038/nrn1327.
12. Pozo, K., and Goda, Y. (2010). Unraveling mechanisms of homeostatic synaptic plasticity. Neuron *66*, 337–351. https://doi.org/10.1016/J.NEURON.2010.04.028.
13. Li, B., Suutari, B.S., Sun, S.D., Luo, Z., Wei, C., Chenouard, N., Mandelberg, N.J., Zhang, G., Wamsley, B., Tian, G., et al. (2020). Neuronal inactivity co-opts LTP machinery to drive potassium channel splicing and homeostatic spike widening. Cell *181*, 1547-1565.e15. https://doi.org/10.1016/j.cell.2020.05.013.
14. Ritzau-Jost, A., Tsintsadze, T., Krueger, M., Ader, J., Bechmann, I., Eilers, J., Barbour, B., Smith, S.M., and Hallermann, S. (2021). Large, stable spikes exhibit differential broadening in excitatory and inhibitory neocortical boutons. Cell Rep *34*, 108612. https://doi.org/10.1016/j.celrep.2020.108612.
15. Zbili, M., Rama, S., Benitez, M.J., Fronzaroli-Molinieres, L., Bialowas, A., Boumedine-Guignon, N., Garrido, J.J., and Debanne, D. (2021). Homeostatic regulation of axonal Kv1.1 channels accounts for both synaptic and intrinsic

modifications in the hippocampal CA3 circuit. Proc Natl Acad Sci U S A *118*. https://doi.org/10.1073/pnas.2110601118.

16. Kim, J., and Tsien, R.W. (2008). Synapse-specific adaptations to inactivity in hippocampal circuits achieve homeostatic gain control while dampening network reverberation. Neuron *58*, 925–937. https://doi.org/10.1016/j.neuron.2008.05.009.
17. Mitra, A., Mitra, S.S., and Tsien, R.W. (2012). Heterogeneous reallocation of presynaptic efficacy in recurrent excitatory circuits adapting to inactivity. Nat Neurosci *15*, 250–257. https://doi.org/10.1038/nn.3004.
18. Castro-Alamancos, M.A., and Connors, B.W. (1997). Distinct forms of short-term plasticity at excitatory synapses of hippocampus and neocortex. Proc Natl Acad Sci U S A *94*, 4161–4166. https://doi.org/10.1073/pnas.94.8.4161.
19. Manahan-Vaughan, D. (2018). Special considerations when using mice for In vivo electrophysiology and long-term studies of hippocampal synaptic plasticity during behavior. Handb Behav Neurosci *28*, 63–84. https://doi.org/10.1016/B978-0-12-812028-6.00003-3.
20. Nguyen, P. V., Duffy, S.N., and Young, J.Z. (2000). Differential maintenance and frequency-dependent tuning of LTP at hippocampal synapses of specific strains of inbred mice. J Neurophysiol *84*, 2484–2493. https://doi.org/10.1152/jn.2000.84.5.2484.
21. Prestigio, C., Ferrante, D., Valente, P., Casagrande, S., Albanesi, E., Yanagawa, Y., Benfenati, F., and Baldelli, P. (2019). Spike-Related Electrophysiological Identification of Cultured Hippocampal Excitatory and Inhibitory Neurons. Mol Neurobiol *56*, 6276–6292. https://doi.org/10.1007/s12035-019-1506-5.
22. Maffei, A., and Turrigiano, G.G. (2008). Multiple modes of network homeostasis in visual cortical layer 2/3. Journal of Neuroscience *28*, 4377–4384. https://doi.org/10.1523/JNEUROSCI.5298-07.2008.
23. Desai, N.S., Rutherford, L.C., and Turrigiano, G.G. (1999). Plasticity in the intrinsic excitability of cortical pyramidal neurons. Nat Neurosci *2*, 515–520. https://doi.org/10.1038/9165.
24. Turrigiano, G.G., Leslie, K.R., Desai, N.S., Rutherford, L.C., and Nelson, S.B. (1998). Activity-dependent scaling of quantal amplitude in neocortical neurons. Nature *391*, 892–896. https://doi.org/10.1038/36103.
25. Hanes, A.L., Koesters, A.G., Fong, M.-F., Altimimi, H.F., Stellwagen, D., Wenner, P., and Engisch, K.L. (2020). Cellular/molecular divergent synaptic scaling of miniature EPSCs following activity blockade in dissociated neuronal cultures. *40*, 4090–4102. https://doi.org/10.1523/JNEUROSCI.1393-19.2020.
26. Frank, C.A., Kennedy, M.J., Goold, C.P.P., Marek, K.W., and Davis, G.W.W. (2006). Mechanisms underlying the rapid induction and sustained expression of synaptic homeostasis. Neuron *52*, 663–677. https://doi.org/10.1016/J.NEURON.2006.09.029.
27. Aoto, J., Nam, C.I., Poon, M.M., Ting, P., and Chen, L. (2008). Synaptic Signaling by All-Trans Retinoic Acid in Homeostatic Synaptic Plasticity. Neuron *60*, 308–320. https://doi.org/10.1016/j.neuron.2008.08.012.
28. Gonzalez Sabater, V., Rigby, M., and Burrone, J. (2021). Voltage-gated potassium channels ensure action potential shape fidelity in distal axons. The Journal of Neuroscience *41*, 5372–5385. https://doi.org/10.1523/jneurosci.2765-20.2021.
29. Hu, H., Shao, L.-R., Chavoshy, S., Gu, N., Trieb, M., Behrens, R., Laake, P., Pongs, O., Knaus, H.G., Ottersen, O.P., et al. (2001). Presynaptic Ca2+-activated K+ channels in glutamatergic hippocampal terminals and their role in spike repolarization and regulation of transmitter release. The Journal of Neuroscience *21*, 9585–9597. https://doi.org/10.1523/JNEUROSCI.21-24-09585.2001.

30. Karmarkar, U.R., and Buonomano, D. V. (2006). Different forms of homeostatic plasticity are engaged with distinct temporal profiles. European Journal of Neuroscience *23*, 1575–1584. https://doi.org/10.1111/j.1460-9568.2006.04692.x.
31. Lee, K.Y., and Chung, H.J. (2014). NMDA receptors and L-type voltage-gated Ca2+ channels mediate the expression of bidirectional homeostatic intrinsic plasticity in cultured hippocampal neurons. Neuroscience *277*, 610–623. https://doi.org/10.1016/j.neuroscience.2014.07.038.
32. Lee, K.Y., Royston, S.E., Vest, M.O., Ley, D.J., Lee, S., Bolton, E.C., and Chung, H.J. (2015). N-methyl-D-aspartate receptors mediate activity-dependent down-regulation of potassium channel genes during the expression of homeostatic intrinsic plasticity. Mol Brain *8*, 1–16. https://doi.org/10.1186/s13041-015-0094-1.
33. Zhao, C.J., Dreosti, E., and Lagnado, L. (2011). Homeostatic synaptic plasticity through changes in presynaptic calcium influx. Journal of Neuroscience *31*, 7492–7496. https://doi.org/10.1523/JNEUROSCI.6636-10.2011.
34. Desai, N.S., Rutherford, L.C., and Turrigiano, G.G. (1999). BDNF regulates the intrinsic excitability of cortical neurons. Learning and Memory *6*, 284–291. https://doi.org/10.1101/lm.6.3.284.
35. Rutherford, L.C., DeWan, A., Lauer, H.M., and Turrigiano, G.G. (1997). Brain-derived neurotrophic factor mediates the activity-dependent regulation of inhibition in neocortical cultures. Journal of Neuroscience *17*, 4527–4535. https://doi.org/10.1523/jneurosci.17-12-04527.1997.
36. Ritzau-Jost, A., Nerlich, J., Kaas, T., Krueger, M., Tsintsadze, T., Eilers, J., Barbour, B., Smith, S.M., and Hallermann, S. (2023). Direct whole-cell patch-clamp recordings from small boutons in rodent primary neocortical neuron cultures. STAR Protoc *4*, 102168. https://doi.org/10.1016/j.xpro.2023.102168.
37. Chipman, P.H., Fetter, R.D., Panzera, L.C., Bergerson, S.J., Karmelic, D., Yokoyama, S., Hoppa, M.B., and Davis, G.W. (2022). NMDAR-dependent presynaptic homeostasis in adult hippocampus: Synapse growth and cross- modal inhibitory plasticity. Neuron *110*, ki. https://doi.org/10.1016/j.neuron.2022.08.014.
38. Niday, Z., and Bean, B.P. (2021). BK channel regulation of afterpotentials and burst firing in cerebellar purkinje neurons. Journal of Neuroscience *41*, 2854–2869. https://doi.org/10.1523/JNEUROSCI.0192-20.2021.
39. Gittis, A.H., Moghadam, S.H., and Du Lac, S. (2010). Mechanisms of sustained high firing rates in two classes of vestibular nucleus neurons: Differential contributions of resurgent Na, Kv3, and BK currents. J Neurophysiol *104*, 1625–1634. https://doi.org/10.1152/jn.00378.2010.
40. Kimm, T., Khaliq, Z.M., and Bean, B.P. (2015). Differential regulation of action potential shape and burst-frequency firing by BK and Kv2 channels in substantia nigra dopaminergic neurons. Journal of Neuroscience *35*, 16404–16417. https://doi.org/10.1523/JNEUROSCI.5291-14.2015.
41. Müller, A., Kukley, M., Uebachs, M., Beck, H., and Dietrich, D. (2007). Nanodomains of single Ca2+ channels contribute to action potential repolarization in cortical neurons. Journal of Neuroscience *27*, 483–495. https://doi.org/10.1523/JNEUROSCI.3816-06.2007.
42. Bock, T., and Stuart, G.J. (2016). The impact of BK channels on cellular excitability depends on their subcellular location. Front Cell Neurosci *10*, 1–8. https://doi.org/10.3389/fncel.2016.00206.
43. Desai, N.S., Cudmore, R.H., Nelson, S.B., and Turrigiano, G.G. (2002). Critical periods for experience-dependent synaptic scaling in visual cortex. Nat Neurosci *5*, 783–789. https://doi.org/10.1038/nn878.

44. Wiesel, T.N., and Hubel, D.H. (1963). Single-cell responses in striate cortex of kittens deprived of vision in one eye. J Neurophysiol *26*, 1003–1017.
45. Wen, W., and Turrigiano, G.G. (2021). Developmental regulation of homeostatic plasticity in mouse primary visual cortex. The Journal of Neuroscience *41*, JN-RM-1200-21. https://doi.org/10.1523/jneurosci.1200-21.2021.
46. Trojanowski, N.F., and Turrigiano, G.G. (2021). CaMKIV signaling is not essential for the maintenance of intrinsic or synaptic properties in mouse visual cortex. eNeuro *8*, 1–12. https://doi.org/10.1523/ENEURO.0135-21.2021.
47. Griffen, T.C., Haley, M.S., Fontanini, A., and Maffei, A. (2017). Rapid plasticity of visually evoked responses in rat monocular visual cortex. PLoS One *12*, 1–12. https://doi.org/10.1371/journal.pone.0184618.
48. Gainey, M.A., Aman, J.W., and Feldman, D.E. (2018). Rapid disinhibition by adjustment of PV intrinsic excitability during whisker map plasticity in mouse S1. Journal of Neuroscience *38*, 4749–4761. https://doi.org/10.1523/JNEUROSCI.3628-17.2018.
49. Maravall, M., Stern, E.A., and Svoboda, K. (2004). Development of intrinsic properties and excitability of layer 2/3 pyramidal neurons during a critical period for sensory maps in rat barrel cortex. J Neurophysiol *92*, 144–156. https://doi.org/10.1152/jn.00598.2003.
50. Breton, J.D., and Stuart, G.J. (2009). Loss of sensory input increases the intrinsic excitability of layer 5 pyramidal neurons in rat barrel cortex. J Physiol *587*, 5107–5119. https://doi.org/10.1113/JPHYSIOL.2009.180943.
51. Sun, Q.Q. (2009). Experience-dependent intrinsic plasticity in interneurons of barrel cortex layer IV. J Neurophysiol *102*, 2955–2973. https://doi.org/10.1152/jn.00562.2009.
52. Li, L., Gainey, M.A., Goldbeck, J.E., and Feldman, D.E. (2014). Rapid homeostasis by disinhibition during whisker map plasticity. Proc Natl Acad Sci U S A *111*, 1616–1621. https://doi.org/10.1073/pnas.1312455111.
53. Jamann, N., Dannehl, D., Lehmann, N., Wagener, R., Thielemann, C., Schultz, C., Staiger, J., Kole, M.H.P., and Engelhardt, M. (2021). Sensory input drives rapid homeostatic scaling of the axon initial segment in mouse barrel cortex. Nat Commun *12*, 1–14. https://doi.org/10.1038/s41467-020-20232-x.
54. Hickmott, P.W. (2005). Changes in intrinsic properties of pyramidal neurons in adult rat S1 during cortical reorganization. J Neurophysiol *94*, 501–511. https://doi.org/10.1152/jn.00924.2004.
55. Francis, H.W., and Manis, P.B. (2000). Effects of deafferentation on the electrophysiology of ventral cochlear nucleus neurons. Hear Res *149*, 91–105. https://doi.org/10.1016/S0378-5955(00)00165-9.
56. Lu, Y., Monsivais, P., Tempel, B.L., and Rubel, E.W. (2004). Activity-dependent regulation of the potassium channel subunits Kv1.1 and Kv3.1. Journal of Comparative Neurology *470*, 93–106. https://doi.org/10.1002/cne.11037.
57. Wang, Y., and Manis, P.B. (2006). Temporal coding by cochlear nucleus bushy cells in DBA/2J mice with early onset hearing loss. JARO - Journal of the Association for Research in Otolaryngology *7*, 412–424. https://doi.org/10.1007/s10162-006-0052-9.
58. Leao, R.N., Berntson, A., Forsythe, I.D., and Walmsley, B. (2004). Reduced low-voltage activated K+ conductances and enhanced central excitability in a congenitally deaf (dn/dn) mouse. J Physiol *559*, 25–33. https://doi.org/10.1113/JPHYSIOL.2004.067421.
59. Him, A., and Dutia, M.B. (2001). Intrinsic excitability changes in vestibular nucleus neurons after unilateral deafferentation. Brain Res *908*, 58–66. https://doi.org/10.1016/S0006-8993(01)02600-2.

60. George, N.M., Gentile Polese, A., Merle, L., Macklin, W.B., and Restrepo, D. (2022). Excitable axonal domains adapt to sensory deprivation in the olfactory system. The Journal of Neuroscience *42*, 1491–1509. https://doi.org/10.1523/JNEUROSCI.0305-21.2021.
61. Barnes, B.Y.C.A., and McNaughton, B.L. (1980). Physiological compensation for loss of afferent synapses in rat hippocampal granule cells during senescence. J. Physiol *309*, 473–485. https://doi.org/10.1113/jphysiol.1980.sp013521ch.
62. Midorikawa, M., and Miyata, M. (2021). Distinct functional developments of surviving and eliminated presynaptic terminals. Proc Natl Acad Sci U S A *118*. https://doi.org/10.1073/pnas.2022423118.
63. O'Leary, T., van Rossum, M.C.W., and Wyllie, D.J.A. (2010). Homeostasis of intrinsic excitability in hippocampal neurones: Dynamics and mechanism of the response to chronic depolarization. Journal of Physiology *588*, 157–170. https://doi.org/10.1113/jphysiol.2009.181024.
64. Pozzi, D., Lignani, G., Ferrea, E., Contestabile, A., Paonessa, F., D'Alessandro, R., Lippiello, P., Boido, D., Fassio, A., Meldolesi, J., et al. (2013). REST/NRSF-mediated intrinsic homeostasis protects neuronal networks from hyperexcitability. EMBO Journal *32*, 2994–3007. https://doi.org/10.1038/emboj.2013.231.
65. Wefelmeyer, W., Cattaert, D., and Burrone, J. (2015). Activity-dependent mismatch between axo-axonic synapses and the axon initial segment controls neuronal output. Proc Natl Acad Sci U S A *112*, 9757–9762. https://doi.org/10.1073/pnas.1502902112.
66. Malik, R., and Chattarji, S. (2012). Enhanced intrinsic excitability and EPSP-spike coupling accompany enriched environment-induced facilitation of LTP in hippocampal CA1 pyramidal neurons. J Neurophysiol *107*, 1366–1378. https://doi.org/10.1152/jn.01009.2011.
67. Valero-Aracama, M.J., Sauvage, M.M., and Yoshida, M. (2015). Environmental enrichment modulates intrinsic cellular excitability of hippocampal CA1 pyramidal cells in a housing duration and anatomical location-dependent manner. Behavioural Brain Research *292*, 209–218. https://doi.org/10.1016/j.bbr.2015.05.032.
68. Kole, M.H.P., Czéh, B., and Fuchs, E. (2004). Homeostatic maintenance in excitability of tree shrew hippocampal CA3 pyramidal neurons after chronic stress. Hippocampus *14*, 742–751. https://doi.org/10.1002/hipo.10212.
69. Kamal, A., Notenboom, R.G.E., De Graan, P.N.E., and Ramakers, G.M.J. (2006). Persistent changes in action potential broadening and the slow afterhyperpolarization in rat CA1 pyramidal cells after febrile seizures. European Journal of Neuroscience *23*, 2230–2234. https://doi.org/10.1111/j.1460-9568.2006.04732.x.
70. Eshra, A., Hirrlinger, P., and Hallermann, S. (2019). Enriched environment shortens the duration of action potentials in cerebellar granule cells. Front Cell Neurosci *13*, 1–9. https://doi.org/10.3389/fncel.2019.00289.
71. Ngodup, T., Goetza, J.A., McGuire, B.C., Sun, W., Lauer, A.M., and Xu-Friedman, M.A. (2015). Activity-dependent, homeostatic regulation of neurotransmitter release from auditory nerve fibers. Proc Natl Acad Sci U S A *112*, 6479–6484. https://doi.org/10.1073/PNAS.1420885112/-/DCSUPPLEMENTAL/PNAS.201420885SI.PDF.
72. Simkin, D., Hattori, S., Ybarra, N., Musia, T.F., Buss, E.W., Richter, H., Matthew Oh, M., Nicholson, D.A., and Disterhoft, J.F. (2015). Aging-related hyperexcitability in CA3 pyramidal neurons is mediated by enhanced A-type K+ channel function and expression. Journal of Neuroscience *35*, 13206–13218. https://doi.org/10.1523/JNEUROSCI.0193-15.2015.
73. Mehranfard, N., Gholamipour-Badie, H., Motamedi, F., Janahmadi, M., and Naderi, N. (2015). Long-term increases in BK potassium channel underlie increased action

potential firing in dentate granule neurons following pilocarpine-induced status epilepticus in rats. Neurosci Lett *585*, 88–91. https://doi.org/10.1016/j.neulet.2014.11.041.

74. Moutin, E., Hemonnot, A.L., Seube, V., Linck, N., Rassendren, F., Perroy, J., and Compan, V. (2020). Procedures for culturing and genetically manipulating murine hippocampal postnatal neurons. Front Synaptic Neurosci *12*, 1–16. https://doi.org/10.3389/fnsyn.2020.00019.

75. Martiszus, B.J., Tsintsadze, T., Chang, W., and Smith, S.M. (2021). Enhanced excitability of cortical neurons in low-divalent solutions is primarily mediated by altered voltage-dependence of voltage-gated sodium channels. Elife *10*, 1–26. https://doi.org/10.7554/eLife.67914.

76. Clements, J.D., and Bekkers, J.M. (1997). Detection of spontaneous synaptic events with an optimally scaled template. Biophys J *73*, 220–229. https://doi.org/10.1016/S0006-3495(97)78062-7.

77. Rothman, J.S., and Silver, R.A. (2018). Neuromatic: An integrated open-source software toolkit for acquisition, analysis and simulation of electrophysiological data. Front Neuroinform *12*, 1–21. https://doi.org/10.3389/fninf.2018.00014.

78. Debanne, D., Boudkkazi, S., Campanac, E., Cudmore, R.H., Giraud, P., Fronzaroli-Molinieres, L., Carlier, E., and Caillard, O. (2008). Paired-recordings from synaptically coupled cortical and hippocampal neurons in acute and cultured brain slices. Nat Protoc *3*, 1559–1568. https://doi.org/10.1038/nprot.2008.147.

79. Gong, Y., Huang, C., Li, J.Z., Grewe, B.F., Zhang, Y., Eismann, S., and Schnitzer, M.J. (2015). High-speed recording of neural spikes in awake mice and flies with a fluorescent voltage sensor. Science (1979) *350*, 1361–1366. https://doi.org/10.1126/science.aab0810.

80. Thevenaz, P., Ruttimann, U.E., and Unser, M. (1998). A pyramid approach to subpixel registration based on intensity. IEEE Transactions on Image Processing *7*, 27–41. https://doi.org/10.1109/83.650848.

81. Brown, L.D., Cai, T.T., and DasGupta, A. (2001). Interval estimation for a binomial proportion. Statistical Science *16*, 101–133.

Figures and legends

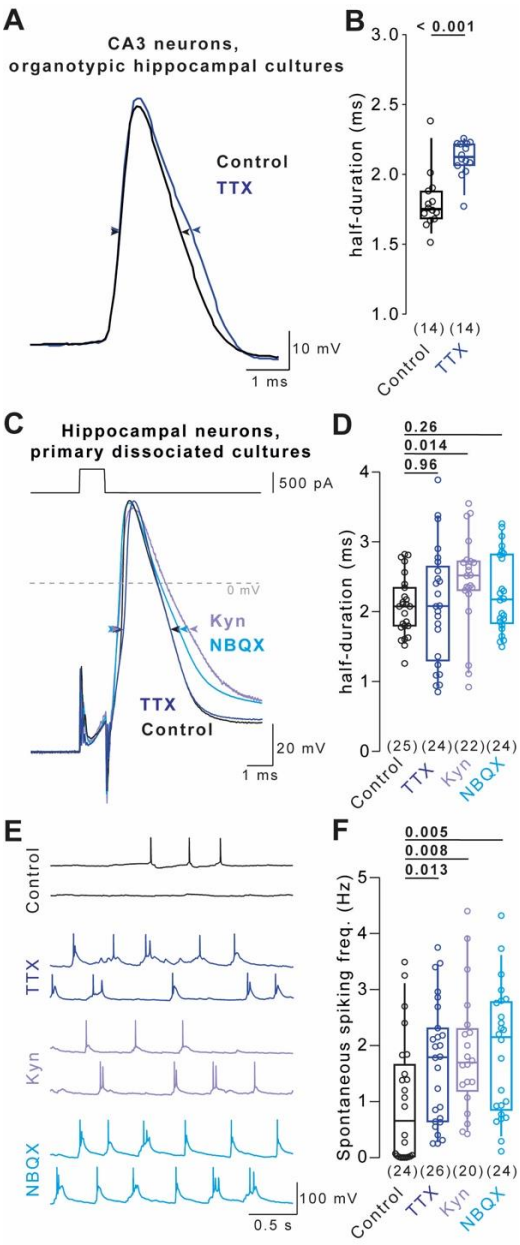

Figure 1 Cell type- and model-specific AP broadening in hippocampal neurons

(A) Example evoked APs recorded from CA3 pyramidal neurons in organotypic hippocampal cultures under control condition (black) and following 48 hours of TTX-treatment (blue).

(B) AP durations recorded under conditions in A.

(C) Example depolarization-evoked APs (500 pA for 1 ms) recorded from neurons in primary dissociated hippocampal cultures under control condition (black) and following 48 hours of TTX- (blue), Kyn- (purple), or NBQX-treatment (turquoise).

(D) AP durations recorded under conditions in C.

(E) Example spontaneous APs recorded under the conditions in C.

(F) Spontaneous AP frequency under the conditions in C.

Numbers in brackets reflect number of recorded neurons. Box plots as median ± interquartile range, whiskers indicate 10–90 percentile. P-values above graphs, significance tested by Mann-Whitney-*U* test.

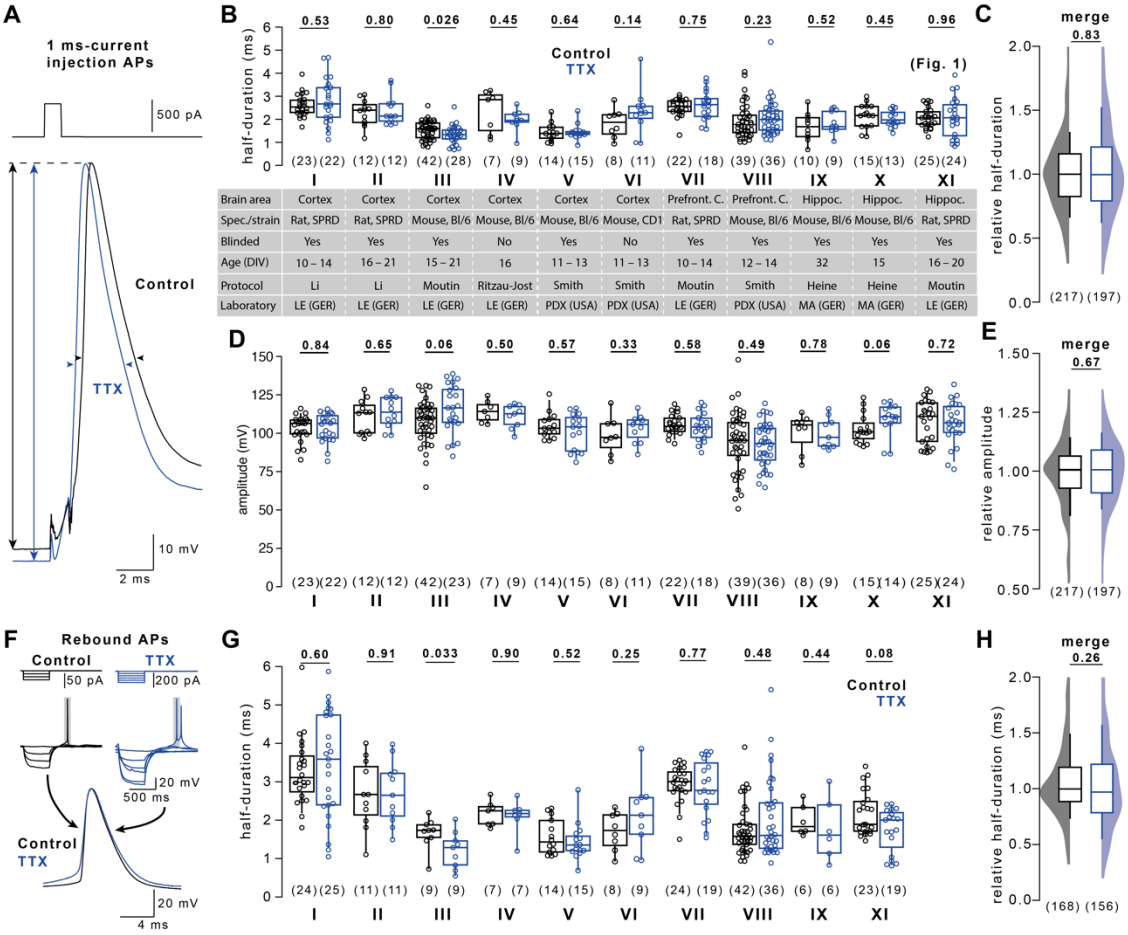

Figure 2 Stable AP duration in primary dissociated neurons during TTX-induced homeostatic plasticity

(A) Example current injection-evoked APs (500 pA for 1 ms) under control condition (black) and following 48 hours of TTX-treatment (blue). AP amplitudes are recorded between the membrane potential preceding the AP and AP peak (arrows), AP durations are recorded at half-maximal amplitude (arrow heads).

(B) AP duration in control and TTX-treated cells (color code as in A) for eleven different experimental conditions (I–XI). Specification of individual conditions is provided in Table S1. Condition XI adopted from Fig. 1D.

(C) Merge of AP durations in control and TTX-treated cells across conditions I–IX normalized to the corresponding condition's control median duration.

(D) AP amplitudes in control and TTX-treated cells as in B.

(E) Cross-conditional merge of AP amplitudes in control and TTX-treated cells as in C.

(F) Example hyperpolarization-evoked "rebound APs" (-150 pA or -60 pA for 500ms) in control and TTX-treated cells (color code as in A).

(G) Rebound AP duration in control and TTX-treated cells as in B.

(H) Cross-conditional merge of normalized durations as in C for rebound APs.

Numbers in brackets reflect number of recorded neurons. Box plots as median ± interquartile range, whiskers indicate 10–90 percentile. P-values provided above graphs; significance tested using Mann-Whitney-*U* tests.

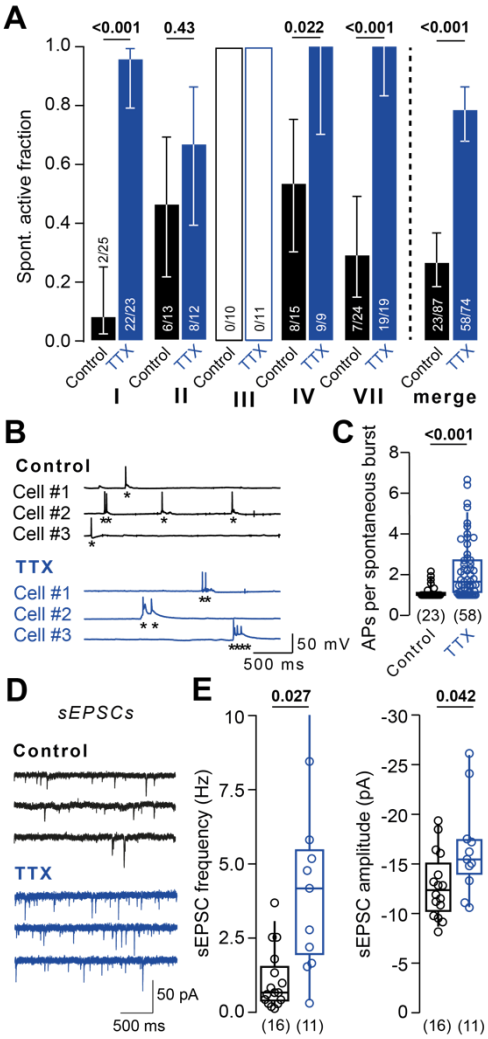

Figure 3 Homeostatic plasticity increases network activity and excitatory synaptic transmission

(A) *Left:* Spontaneously active control (black) and TTX-treated cells (blue) in condition I–IV and VII. *Right*: Active neurons merged across conditions I–IV and VII.

(B) Example spontaneous AP bursts in control and TTX-treated cells. Asterisks mark individual APs.

(C) AP number per burst in control and TTX-treated cells across conditions I–IV and VII.

(D) Example spontaneous excitatory postsynaptic currents (sEPSCs) in control and TTX-treated cells.

(E) *Left:* sEPSC frequency and *Right:* sEPSC amplitude in control recordings and after TTX-treatment (merged data from conditions I and II).

Numbers in brackets reflect number of recorded neurons. Bars in A reflect fraction of spontaneously active neurons. Whiskers in A reflect confidence limits for 95% confidence interval based on Wilson interval. Box plots as median ± interquartile range, whiskers indicate 10–90 percentile. P-values above graphs, significance tested by Fisher's exact test in A or Mann-Whitney-*U* test elsewhere.

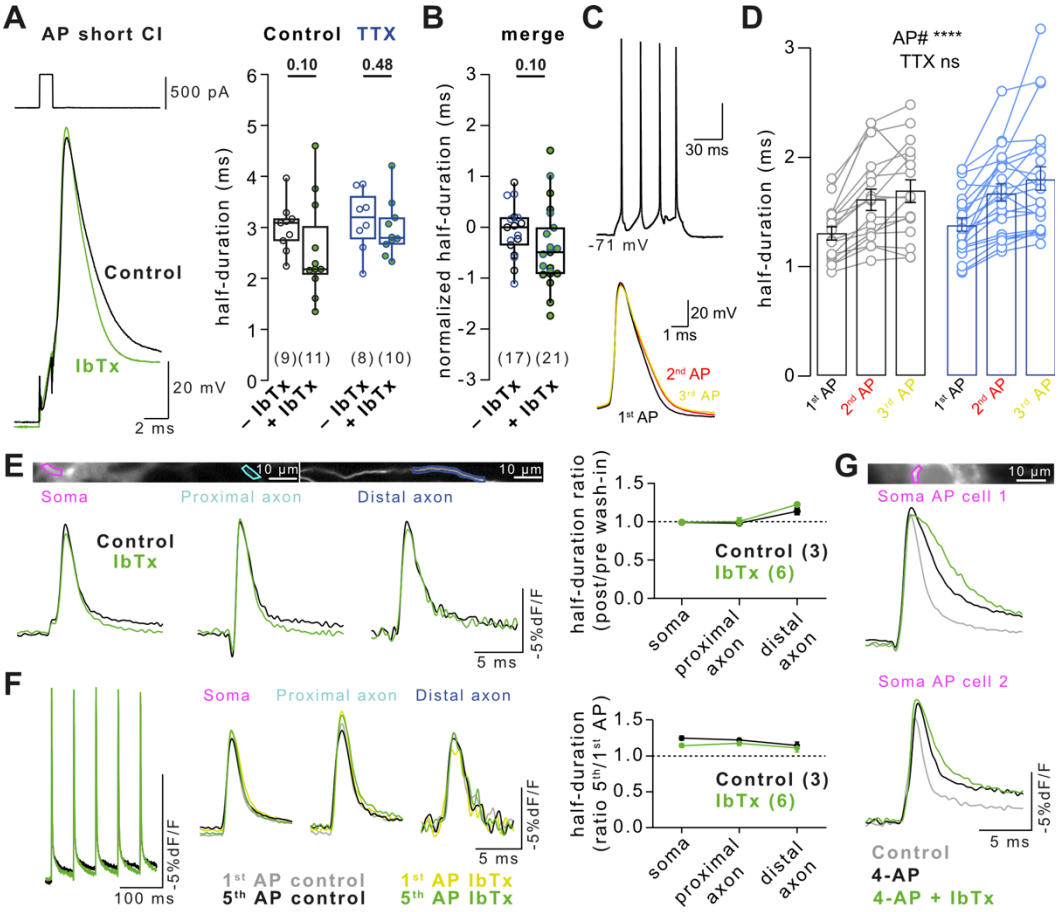

Figure 4 Lack of BK channel-dependent AP broadening in dissociated cultured neurons

(A) *Left:* Example current injection-evoked APs (500 pA for 1 ms) in control solution (black) and solution containing 300 nM Iberiotoxin (IbTx, green). *Right:* AP duration in control and TTX-treated cells recorded IbTx-free (black and blue, respectively) or IbTx-containing solution (green). Data recorded under condition I.

(B) Merged AP duration across control and TTX-treated cells for recordings in IbTx-free and IbTx-containing solution (data in A normalized to the respective group's median duration in control solution).

(C) APs evoked by a 200 ms current injection (top) and overlay of the forst three evoked APs (bottom).

(D) Broadening of AP duration of the 3 first APs during 200 ms current injections in control (black, *left*) and TTX-treated cells (blue, *right*). Bars as mean ± SEM, lines with markers depict recordings from individual neurons.

(E) *Left:* Example Ace-mNeon-recorded somatic, proximal axonal, and distal axonal APs in a primary hippocampal cultured neuron in IbTx-free solution (black) and

following BK channel block by IbTx (100 nM, green). *Right:* Ratio of somatic and axonal AP durations in IbTx-free and IbTx-containing solution.

(F) *Left:* Example AP train (5 x 20 Hz) and overlay of 1st and 5th train AP at the soma, proximal, and distal axon in control condition (grey and black) and following BK channel block by IbTx (yellow and green). *Right:* AP broadening (ratio of 5th over 1st train AP duration) in the three compartments in control and IbTx-containing solution.

(G) Somatic APs under control condition (grey), following treatment with 4-AP (black), and following treatment with 30µM 4-AP + 100 nM IbTx (green).

Numbers in brackets reflect number of recorded neurons. Box plots as median ± interquartile range, whiskers indicate 10–90 percentile. Plots in D–F as mean ± SEM. P-values above graphs, significance tested by Mann-Whitney-*U* test.

Figure supplements

Group	Species	Strain	Brain area	Culture age (days *in vitro*)	Lab which recordings were performed at	External recor-ding solution	External [Ca^{2+}] (mM)	Internal recording solution	Growth medium	Protocol Reference
I	Rat	Sprague-Dawley	Cortex	10–14	Hallermann Lab, Leipzig (Germany)	1.)	2.0	5.)	NbActiv4	Li *et al.*, Cell 2020
II	Rat	Sprague-Dawley	Cortex	16–21	Hallermann Lab, Leipzig (Germany)	1.)	2.0	5.)	NbActiv4	Li *et al.*, Cell 2020
III	Mouse	C57BL/6N	Cortex	15–20	Hallermann Lab, Leipzig (Germany)	2.)	1.1	6.)	BrainPhys	Moutin *et al.*, Front. Synaptic Neurosci 2020
IV	Mouse	C57BL/6N	Cortex	16	Hallermann Lab, Leipzig (Germany)	2.)	1.1	6.)	MEM, 5% serum + supplements	Ritzau-Jost *et al.*, Cell Reports 2021
V	Mouse	C57BL/6J	Cortex	11–13	Smith Lab, Portland (OR, USA)	3.)	2.0	7.)	MEM, 5% serum + supplements	Martiszus BJ *et al.*, eLife 2021
VI	Mouse	CD1	Cortex	11–13	Smith Lab, Portland (OR, USA)	3.)	2.0	7.)	MEM, 5% serum + supplements	Martiszus BJ *et al.*, eLife 2021
VII	Rat	Sprague-Dawley	Pre-frontal cortex	10–14	Hallermann Lab, Leipzig (Germany)	1.)	2.0	5.)	BrainPhys	Moutin *et al.*, Front. Synaptic Neurosci 2020
VIII	Mouse	C57BL/6J	Pre-frontal cortex	10–14	Smith Lab, Portland (OR, USA)	1.)	2.0	8.)	MEM, 5% serum + supplements	Martiszus BJ *et al.*, eLife 2021
IX	Mouse	C57BL/6N	Hippo-campus	32	Heine Lab, Mainz (Germany)	4.)	2.0	9.)	Neurobasal A+ supplements	Li *et al.*, Cell 2020
X	Mouse	C57BL/6J	Hippo-campus	15	Heine Lab, Mainz (Germany)	4.)	2.0	9.)	Neurobasal A + supplements	Li *et al.*, Cell 2020
XI	Rat	Sprague-Dawley	Hippo-campus	16–20	Hallermann Lab, Leipzig (Germany)	1.)	2.0	5.)	BrainPhys	Moutin *et al.*, Front. Synaptic Neurosci 2020

1.) 122 NaCl, 3 KCl, 10 Glucose, 26 $NaHCO_3$, 2 $CaCl_2$, 1.3 $MgCl_2$, 1.25 NaH_2PO_4
2.) 125 NaCl, 3 KCl, 25 Glucose, 25 $NaHCO_3$, 1.1 $CaCl_2$, 1.1 $MgCl_2$, 1.25 Na_2HPO_4
3.) 150 NaCl, 4 KCl, 10 Glucose, 10 HEPES, 2 $CaCl_2$, 1 $MgCl_2$
4.) 145 NaCl, 2.5 KCl, 24 Glucose, 10 HEPES, 2 $CaCl_2$, 1.3 $MgCl_2$
5.) 130 K gluconate, 10 HEPES, 1 $MgCl_2$, 0.3 EGTA, 4 Mg-ATP, 0.3 Na-GTP, 10 Tris-Phosphocreatine
6.) 150 K gluconate, 10 K-HEPES, 10 NaCl, 0.05 EGTA, 3 Mg-ATP, 0.3 Na-GTP
7.) 135 K gluconate, 10 HEPES, 4 NaCl, 0.05 EGTA, 3 Na_2ATP, 0.3 NaGTP, 3 $MgCl_2$, 10 Na_2-Creatine phosphate
8.) 130 K gluconate, 10 HEPES, 0.3 EGTA, 4 Na_2ATP (or Mg-ATP), 0.3 NaGTP, 2 $MgCl_2$, 10 Na_2-Creatine phosphate (or Tris-Creatinine phosphate)
9.) 140 K gluconate, 20 HEPES, 2 NaCl, 0.5 EGTA, 4 Na_2ATP, 0.3 NaGTP, 3 $MgCl_2$

Figure 2 – figure supplement 1

Additional information on recording conditions

The table lists additional relevant information on the experimental conditions I – XI.

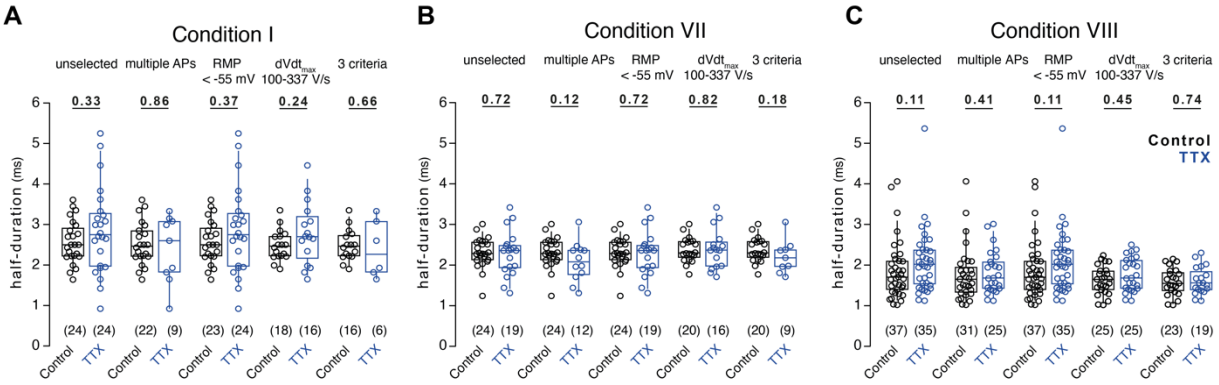

Figure 2 – figure supplement 2

Absence of TTX-induced AP broadening in further selected conditions

(A) Box plots of AP durations under control condition (black) or upon TTX-treatment (blue) recorded in condition I either unselected or selected for parameters reflecting unimpaired neuronal function.

(B) AP durations as in A for recordings in condition VII.

(C) AP durations as in A for recordings in condition VIII.

Numbers of recorded neurons provided in brackets. Box plots depict median ± interquartile range, whiskers reflect 10–90 percentile. P-values calculated by Mann-Whitney-*U* test.

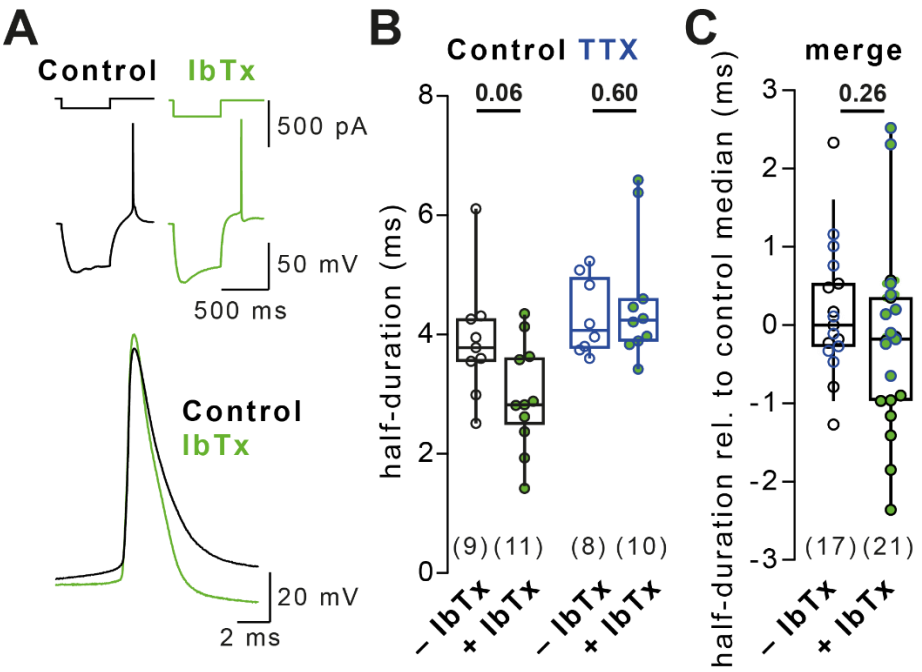

Figure 4 – figure supplement 1

BK channel block does not affect rebound AP duration

(A) Example rebound APs in control solution (black) and solution containing 300 nM Iberiotoxin (IbTx, green).

(B) AP duration in control and TTX-treated cells in IbTx-free (black and blue, respectively) or IbTx-containing solution (green). Data recorded in condition I.

(C) Merged AP duration across control and TTX-treated cells for recordings in IbTx-free and IbTx-containing solution (data in A, normalized to the respective group's median duration in IbTx-free solution).

Numbers of recorded neurons provided in brackets. Box plots depict median ± interquartile range, whiskers reflect 10–90 percentile. P-values calculated by Mann-Whitney-*U* test.